ISSN 1392-1207. MECHANIKA. Vol. 31, No. 6, 2025: 578–588

Optimization Design Method of High-Speed Angular Contact Ball Bearings

Ye JI*,******, Kun HUANG**, Haotian ZHENG***, Yanchun LI****, Dongfeng WANG*****, Congying GAO******, Duanduan SUN*******

**School of Artificial Intelligence, Luoyang Institute of Science and Technology, Luoyang 471023, China, E-mail: ji2000ye@126.com*
***Luoyang Bearing Research Institute Co., Ltd., Luoyang 471039, China, E-mail: 13653873677@126.com*
****Luoyang Bearing Research Institute Co., Ltd., Luoyang 471039, China, E-mail: 15036989086@163.com*
*****Luoyang Bearing Research Institute Co., Ltd., Luoyang 471039, China, E-mail: 13525443494@139.com*
******Luoyang Bearing Science & Technology Co., Ltd., Luoyang 471033, China, E-mail: zyswdf@163.com*
*******Luoyang Bearing Research Institute Co., Ltd., Luoyang 471033, China, E-mail: 317662561@qq.com*
********Luoyang Juchuang Bearing Technology Co., Ltd., Luoyang 471003, China, E-mail: duan706009512@126.com*
*********Henan Key Laboratory of Green Building Materials Manufacturing and Intelligent Equipment, Luoyang 471023, China, E-mail: ji2000ye@126.com*

https://doi.org/10.5755/j02.mech.41155

Nomenclature

f_i – curvature coefficient of inner ring raceway; f_e – curvature coefficient of outer ring raceway; D_w – ball diameter; α – contact angle after applying pre-tightening force; $\Delta\alpha$ – variation of contact angle; d – inner diameter; F_a – axial preload; i – number of rolling element columns; ω_{im} – angular velocity of the inner ring relative to the cage; v_A^b – linear velocity of the ball relative to the cage (at point A); v_A^t – linear velocity of raceway surface relative to cage (at point A); ω_i – angular velocity of the inner ring; n_m – rotational speed of the ball with the cage; F_1 – spin-roll ratio; Q – the force between a single ball and raceway under preload; Q_n – the normal force between a single ball and the raceway under preload; Q_e – contact force between the outer ring and the ball; Q_{ea} – the axial component of Q_e; Q_{er} – the radial component of Q_e; Q_i – Contact force between the inner ring and the ball; Q_{ia} – the axial component of Q_i; Q_{ir} – the radial component of Q_i; D – outer diameter; K_d – dynamic stiffness; δ_1 – axial displacement caused by applying F_a; ω_{em} – angular velocity of the outer ring relative to the cage; ω_{bi} – angular velocity of the rotating shaft of the ball relative to the inner ring through the contact points A and O_1; ω_{be} – angular velocity of the rotating shaft of the ball relative to the outer ring through the contact points B and O_1; d_m – pitch circle diameter; α_i – contact angle between ball and inner ring; β – space attitude angle of ball rotation axis; α_e – contact angle between ball and outer ring; ω_m – angular velocity of the ball with the cage; ω_{bi}^s – spin component of ball relative to inner raceway; ω_{bi}^R – rolling of ball relative to inner raceway; ω_{be}^s – spin component of ball relative to outer raceway; ω_{be}^R – rolling of ball relative to outer raceway; δ – normal deflection; α^0 – initial contact angle; K_n – total load-deformation constant between the ball and the inner or outer rings; $K_{i(e)}$ – load-deformation constant between the ball and the inner (outer) ring; η – elastic constant of the contact between the ring and the ball; E_1, E_2 – elastic modulus of the material of the parts in contact with each other; μ_1, μ_2 – Poisson's ratio of the material of the parts in contact with each other; F_c – centrifugal force of a ball; N – number of balls; K_s – static stiffness; δ_2 – axial displacement caused by F_c; δ_a – axial displacement.

1. Introduction

High-speed ACBBs are widely used in aerospace engines, high-performance machine tools, and other precision equipment to ensure operational accuracy and stability. However, current design methodologies for ACBBs remain inadequate. This study focuses on existing optimization objectives by establishing a dynamic stiffness model and incorporating it as an additional optimization target. The research systematically analyzes the correlation be-tween variations in key ACBBs design parameters and the respective optimization objective functions.

The optimization design of rolling bearings is a multi-objective problem, and there is almost no design scheme that makes all targets optimal. The improvement of one target performance often needs to reduce the performance of other targets. Deb proposed a non-dominated sorting genetic algorithm NSGA-II, which can better solve the multi-objective optimization design problem [1]. Choi et al. used genetic algorithm to optimize the bearing structure parameters with the longest life as the objective function [2]. Gupta et al. used the NSGA II genetic algorithm to carry out multi-objective optimization design of the rated dynamic load, rated static load and oil film thickness of the rolling bearing, and studied the sensitivity of the structural parameters such as the curvature radius coefficient of the inner ring raceway and the ball diameter [3].

In China, bearing optimization design has been paid great attention in recent decades. Li et al. used the NSGA II method to optimize the design with the goal of rated dynamic load and rated static load [4]. Cui et al. conducted multi-objective optimization design based on NSGA II genetic algorithm to analyze the influence of structural parameters on the dynamic performance of bearings with the goal of rated dynamic load, bearing stiffness and spin-roll ratio [5]. Wu transformed the analy-

sis of rotation slip of high-speed angular contact ball bearings into the analysis of spin-roll ratio, and obtained the variation law of spin-roll ratio of high-speed angular contact ball bearings under different working conditions or different bearing parameters and the relationship between spin-roll ratio and various parameters [6]. Yang et al. established a quasi-dynamic calculation model, and analyzed the relationship between the main parameters of the bearing and the optimization objective with the spin-roll ratio, axial stiffness and rated dynamic load as the optimization objectives [7]. Liu et al. optimized the pitch diameter, ball diameter, ball number, inner ring raceway curvature coefficient and outer ring raceway curvature coefficient of bearing ball set with the objective function of rotation-rolling ratio, basic rated dynamic load, friction torque and axial stiffness [8].

The variation law of bearing stiffness, especially dynamic stiffness, remains to be discussed. Due to the complexity of dynamic stiffness, the existing design method does not promote the optimization goal of dynamic stiffness. Yun et al. proposed a method to measure the dynamic support stiffness of spindle online by means of synchronous excitation. By studying the angle relationship between the residual vibration displacement and the excitation response displacement, the dynamic support stiffness test principle is derived [9]. Luo et al. derived the expression of axial stiffness of angular contact ball bearings, established an objective function with bearing stiffness as the optimization objective, and optimized the design of angular contact ball bearings [10]. Wang et al. based on the 5-degree-of-freedom quasi-static model of the channel control theory, theoretically solved the static stiffness and dynamic stiffness of the bearing using different stiffness analytical methods, and verified the correctness of the model by comparing with the reference value [11]. Based on the theory of elastic mechanics, rolling bearing dynamics and channel control theory, Wang et al. calculated the radial displacement of the inner ring of angular contact ball bearing under centrifugal force, and gave the calculation method and corresponding program of the contact stiffness between the rolling element of high-speed angular contact ball bearing and the inner and outer rings and the overall radial stiffness, axial stiffness and angular stiffness of the bearing when considering the influence of the centrifugal displacement of the inner ring [12].

Recently, Singh et al. proposed a method that integrates genetic algorithm (GA) and grid search method (GSM) to design and optimize the internal geometry of angular contact ball bearings (ACBBs), with the dynamic capacity as the optimization objective [13]. Abbas introduced a novel approach for optimizing rolling element bearings design and lubricant selection utilizing electrohydrodynamic lubrication (EHL) theory. First, a Multi-Objective Optimization (MOO) was formulated, using a Non-dominated Sorting Genetic Algorithm (NSGA-II), to generate Pareto front optimal designs, capturing the trade-off between the two objective functions, namely maximizing minimum film thickness and minimizing the total friction torque. Second, a machine learning model was trained using the results obtained from the NSGA-II model. The machine learning algorithm used in this article was Random Forest Regression (RFR), a supervised ensemble learning method combining multiple decision trees to improve predictive accuracy [14]. Baklouti et al. determined the most efficient internal geometric parameters of the rolling bearing by introducing the uncertainty of the internal geometric parameters of the bearing and incorporating bearing reliability into the optimization algorithm [15].

Research on bearing design optimization remains inadequate. Based on the operating condition requirements of high-speed ACBBs, the optimization objectives are studied. The spin-roll ratio and rated dynamic load of ACBBs are usually optimization goals, and sometimes static stiffness is increased. This study comprehensively considers the spin-roll ratio, rated dynamic load, static stiffness and dynamic stiffness, analyzes the variation of the main design parameters and these indicators, and provides a basis for the optimization design of high-speed ACBBs.

2. Methodology

2.1. Kinematics analysis of high-speed ACBB

When an ACBB operates at high speeds, the balls experience significant centrifugal force, causing them to be in an ‘outward-thrown’ state, pressing tightly against the outer ring. It is assumed that the balls are controlled by the outer raceway, meaning there is pure rolling (no sliding) between the balls and the outer raceway, and the linear velocities of the two surfaces at the contact point are equal. For kinematic analysis, the coordinate system established for the ball and its motion analysis are illustrated in Fig. 1, where the solid circular line represents the ball. Point A is in contact with the inner ring, and point B is in contact with the outer ring.

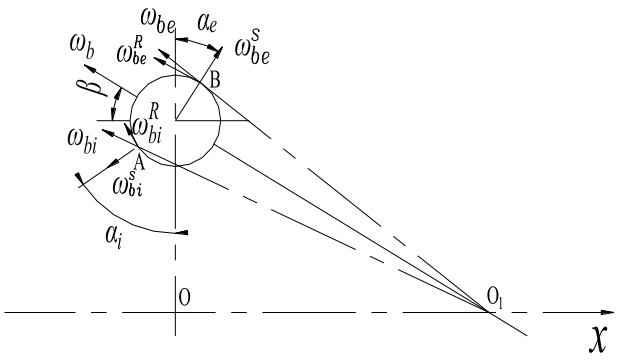

Fig. 1 Analysis of ball motion about ACBB

The outer ring is fixed, the inner ring rotating forward around the x-axis at a speed of n_i, the cage rotating around the x-axis with the ball at a speed of n_m, and the direction being the same as the inner ring. On the one hand, the ball rotates around the x-axis with the cage, and at the same time rotates around its own axis relative to the moving system. The angular velocity (rotational speed) is $\omega_b(n_b)$, and the direction of ω_b is shown in Fig. 1. To obtain the linear velocity at point A, the geometric relationship with ω_b is further analyzed, as shown in Fig. 2.

Draw a straight line through point A parallel to ω_b. With the center of the ball at O_2, draw a horizontal line through O_2 that intersects the line parallel to ω_b through point A at point A_4. Then, draw a vertical line through O_2 that intersects line A_4A at point A_1. Based on the geometric

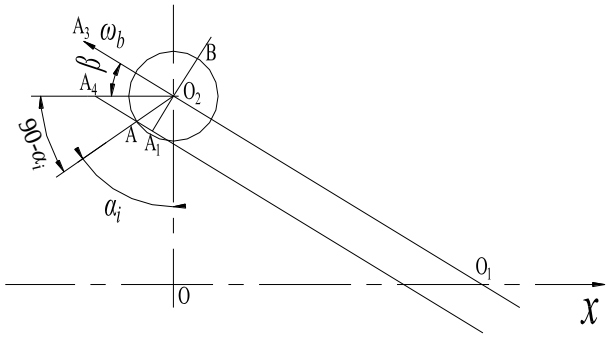

Fig. 2 Geometric relationship at point A with respect to ω_b

conditions in the Fig. 2, we obtain $\angle AO_2A_1 = \alpha_i - \beta$. At the contact point A, the linear velocities of the ball and the channel surface relative to the cage are

$$v_A^b = 0.5\omega_b D_w \cos\left(\angle AO_2A_1\right) \tag{1}$$

The distance from O_2 to the x-axis is $0.5d_m$, and the distance from point A to line O_2A_4 is $0.5D_w\cos\alpha_i$. This leads to the following relation

$$v_A^t = 0.5\omega_{im} d_m \left(1-\gamma_i\right) \tag{2}$$

When the ball does not slip, there is

$$v_A^b = v_A^t \tag{3}$$

The equation can be obtained

$$\omega_b = \omega_{im} \frac{d_m\left(1-\gamma_i\right)}{D_w \cos\left(\alpha_i - \beta\right)} \tag{4}$$

Similar to the analysis at point A, for point B, there exists

$$\omega_b = \omega_{em} \frac{d_m\left(1+\gamma_e\right)}{D_w \cos\left(\alpha_e - \beta\right)}, \tag{5}$$

where

$$\gamma_i = \frac{D_w \cos\alpha_i}{d_m}, \tag{6}$$

$$\gamma_e = \frac{D_w \cos\alpha_e}{d_m}. \tag{7}$$

The inner ring rotates relative to the cage, and the speed vector is

$$\omega_{im} = \omega_i - \omega_m. \tag{8}$$

The direction is the same as ω_i. The outer ring is stationary, and the speed vector relative to the cage is

$$\omega_{em} = -\omega_m, \tag{9}$$

$$\omega_b = \frac{d_m}{D_w}\omega_i \times \times \frac{\left(1-\gamma_i\right)\left(1+\gamma_e\right)}{\left(1-\gamma_i\right)\cos\left(\alpha_e-\beta\right)+\left(1+\gamma_e\right)\cos\left(\alpha_i-\beta\right)}, \tag{10}$$

$$n_b = \frac{d_m}{D_w} n_i \times \times \frac{\left(1-\gamma_i\right)\left(1+\gamma_e\right)}{\left(1-\gamma_i\right)\cos\left(\alpha_e-\beta\right)+\left(1+\gamma_e\right)\cos\left(\alpha_i-\beta\right)}. \tag{11}$$

The angular velocity and rotational speed of the ball revolution are

$$\omega_m = \frac{\omega_i\left(1-\gamma_i\right)\cos\left(\alpha_e-\beta\right)}{\left(1+\gamma_e\right)\cos\left(\alpha_i-\beta\right)+\left(1-\gamma_i\right)\cos\left(\alpha_e-\beta\right)}, \tag{12}$$

$$n_m = \frac{n_i\left(1-\gamma_i\right)\cos\left(\alpha_e-\beta\right)}{\left(1+\gamma_e\right)\cos\left(\alpha_i-\beta\right)+\left(1-\gamma_i\right)\cos\left(\alpha_e-\beta\right)}. \tag{13}$$

The spin component and the rolling component of the relative channel of the sphere are

$$\omega_{bi}^s = \omega_{im}\sin\alpha_i + \omega_b \sin\left(\alpha_i-\beta\right), \tag{14}$$

$$\omega_{bi}^R = \omega_{im}\cos\alpha_i + \omega_b \cos\left(\alpha_i-\beta\right), \tag{15}$$

$$\omega_{be}^s = \omega_{em}\sin\alpha_e - \omega_b \sin\left(\alpha_e-\beta\right), \tag{16}$$

$$\omega_{be}^R = -\omega_{em}\cos\alpha_e + \omega_b \cos\left(\alpha_e-\beta\right). \tag{17}$$

At high speed, the spin component between the ball and the outer raceway is 0, which is controlled by the outer raceway and satisfies the equation

$$\tan\beta = \frac{\cos\alpha_e \sin\alpha_e}{\cos^2\alpha_e + \gamma_e}. \tag{18}$$

The derivation process refers to Reference [16].

2.2. Spin-roll ratio analysis of high-speed ACBB

Through the above analysis, when ACBB moves at high speed, it is appropriate to use the comparison between the spin component and the rolling component of the ball relative to the inner channel, which is also the main reason for friction and heating under high speed conditions. The spin-roll ratio is expressed as

$$F_1 = \frac{\omega_{bi}^s}{\omega_{bi}^R} = \gamma_i \tan\alpha_i + \left(1-\gamma_i\right)\tan\left(\alpha_i-\beta\right). \tag{19}$$

2.3. Rated dynamic load analysis of high-speed ACBB

There are two kinds of bearing life calculation methods in the world. One is the working capacity coefficient method based on the early bearing theory of A. Palmgen in Sweden. The other is based on the rated dy-

namic load method proposed by A. Palmgren et al. in the later period. The International Organization for Standardization (ISO) began to use the rated dynamic load method to calculate the bearing life in 1959. According to the national standard, the rated dynamic load calculation formula is

$$C_r = b_m f_c \left(i\cos\alpha\right)^{0.7} N^{\frac{2}{3}} D_w^{1.8},\ D_w \le 25.4 \text{ mm}, \quad (20)$$

$$C_r = 3.647 b_m f_c \left(i\cos\alpha\right)^{0.7} N^{\frac{2}{3}} D_w^{1.4},\ D_w > 25.4 \text{ mm}. \quad (21)$$

The coefficient b_m represents the type coefficient of the bearing. When there is a filling raceway, its value is 1.1. The value of radial contact and angular contact ball bearings, as well as spherical ball bearings and outer spherical bearings, is 1.3. The coefficient f_c is found according to the standard [17].

The method of Reference [7] has been applied to the design file of Luoyang Bearing Research Institute Co., Ltd., the file name being represented by ZYB, and the rated dynamic load calculation formula is

$$C_r = f_c F\left(D_w\right) N^{\frac{2}{3}} \cos^{0.7}\alpha, \quad (22)$$

whereas

$$f_c = \frac{37.9 b_m \gamma^{0.3}\left(1-\gamma\right)^{1.39}}{\left(1+\gamma\right)^{\frac{1}{3}}} \times \left(\frac{2f_i}{2f_i-1}\right)^{0.41} \times \left[1+1.14\left(\frac{1-\gamma}{1+\gamma}\right)^{5.73} \times \left(\frac{f_i}{f_e} \times \frac{2f_e-1}{2f_i-1}\right)^{1.37}\right]^{-0.3}, \quad (23)$$

$$F(D_w) = \begin{cases} D_w^{1.8}, & D_w \le 25.4, \\ 3.647 D_w^{1.4}, & D_w > 25.4. \end{cases} \quad (24)$$

The difference between the two is mainly the calculation of f_c. The former needs to calculate $\left(D_w \cos\alpha\right)/d_m$ and look up the table to determine the value; the latter is an analytical formula related to f_i, f_e and γ.

2.4. Dynamic(static) stiffness analysis of high-speed ACBB

ACBB-stiffness measurement generally only loads axial preload, and the contact angle increases when subjected to axial load. The contact deformation of the ball and the two rings at any position after the force is δ, which is equal to the deformation of the distance between the m-point and the n-point of the curvature center of the inner and outer raceways, as shown in Fig. 3.

The normal contact load between the ball and the raceway satisfies

$$Q_n = K_n \delta^{1.5} \quad (25)$$

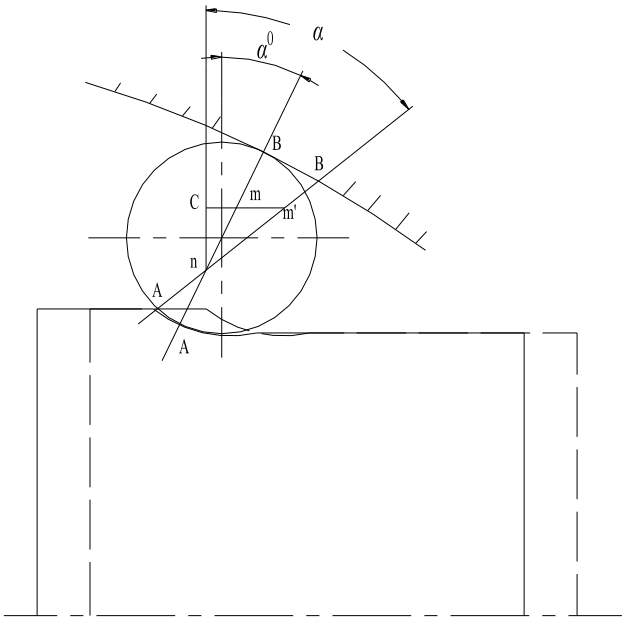

Fig. 3 Change in ACBB contact angle under axial load

It can be seen from Fig. 2

$$nm' = nm + \delta = BD_w + \delta, \quad (26)$$

where B is

$$B = f_i + f_e - 1 \quad (27)$$

$$nc = nm\cos\alpha^0 = nm'\cos\alpha \quad (28)$$

$$\frac{\cos\alpha^0}{\cos\alpha} = \frac{BD_w + \delta}{BD_w}. \quad (29)$$

Therefore,

$$\delta = BD_w\left(\frac{\cos\alpha^0}{\cos\alpha} - 1\right). \quad (30)$$

Substituting Eq. (30) into Eq. (25), we get

$$Q_n = K_n \left(BD_w\right)^{1.5}\left(\frac{\cos\alpha^0}{\cos\alpha} - 1\right)^{1.5}. \quad (31)$$

ACBB is only subjected to axial preload. The load of each rolling element is evenly distributed, and the resultant force is

$$Q = \frac{F_a}{N}. \quad (32)$$

According to the parallelogram rule, it can be obtained

$$Q_n = Q\sin\alpha \quad (33)$$

According to Eqs. (31)-(33), it can be derived that

$$\frac{F_a}{NK_n\left(BD_w\right)^{1.5}}=\frac{\left(\frac{\cos\alpha^0}{\cos\alpha}-1\right)^{1.5}}{\sin\alpha}. \tag{34}$$

K_n is denoted by

$$K_n=\frac{1}{\left[\left(\frac{1}{K_e}\right)^{\frac{1}{n}}+\left(\frac{1}{K_i}\right)^{\frac{1}{n}}\right]^n}, \tag{35}$$

K_i and K_e are denoted by

$$K_{i,e}=\left(\frac{39}{9n_\delta^3\eta^2\Sigma\rho}\right)^{0.5}, \tag{36}$$

where

$$\Sigma\rho=\rho_{1\mathrm{I}}+\rho_{1\Pi}+\rho_{2\mathrm{I}}+\rho_{2\Pi}. \tag{37}$$

Here $\rho_{1\mathrm{I}}$, $\rho_{1\Pi}$, $\rho_{2\mathrm{I}}$ and $\rho_{2\Pi}$ are expressed as:

$$\rho_{1\mathrm{I}}=\frac{2}{D_w}, \tag{38}$$

$$\rho_{1\Pi}=\frac{2}{D_w}, \tag{39}$$

$$\rho_{2\mathrm{I}}=-\frac{1}{f_iD_w}, \tag{40}$$

$$\rho_{2\Pi}=\frac{2\gamma}{D_w\left(1-\gamma\right)}. \tag{41}$$

γ is denoted by

$$\gamma=\frac{D_w\cos\alpha}{d_m}. \tag{42}$$

According to the calculation results of Eq. (43), the value of n_δ is determined by referring to Table 6-1 in Reference [18].

$$F\left(\rho\right)=\frac{\left(\rho_{1\Pi}-\rho_{1\mathrm{I}}\right)+\left(\rho_{2\Pi}-\rho_{2\mathrm{I}}\right)}{\Sigma\rho} \tag{43}$$

The elastic constant of the contact between the ring and the ball is expressed as

$$\eta=\frac{1-\mu_1^2}{E_1}+\frac{1-\mu_2^2}{E_2} \tag{44}$$

After high-speed rotation of the bearing, the working state of ACBB is shown in Fig. 4.

The centrifugal force of the ball is

$$F_c=2.26\times10^{-11}d_mD_w^3n_m^2. \tag{45}$$

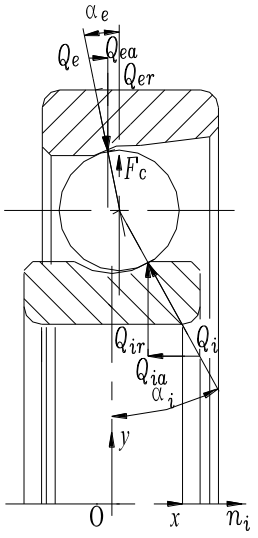

Fig. 4 ACBB working status

Q_e and Q_i can be decomposed into axial load and radial load. According to the force balance equation, the equation is satisfied

$$Q_{ia}=Q_{ea}, \tag{46}$$

$$Q_{ir}+F_c=Q_{er}, \tag{47}$$

whereas

$$Q_{ia}=\frac{F_a}{N}. \tag{48}$$

According to the equilibrium relationship, it can be obtained

$$Q_{ia}\cot\alpha_i+F_c=Q_{er}. \tag{49}$$

Furthermore, it is deduced that

$$\cot\alpha_e=\cot\alpha_i+\frac{F_c}{Q_{ia}}. \tag{50}$$

It can be approximately considered that the variation of contact angle satisfies

$$\alpha_e=\alpha-\Delta\alpha, \tag{51}$$

$$\alpha_i=\alpha+\Delta\alpha. \tag{52}$$

The outer ring is fixed. Under the action of F_a, the displacement of the inner ring of the bearing at high speed is divided into two parts. The first part is the axial component of the normal displacement generated after applying F_a, that is

$$\delta_1=\delta\sin\alpha. \tag{53}$$

After the inner ring rotates, due to the increase of centrifugal force, the axial displacement δ_2 is

$$\delta_2=\delta_i\sin\alpha_i+\delta_e\sin\alpha_e \tag{54}$$

whereas

$$\delta_{i,e}=\left(\frac{Q_{i,e}}{K_{i,e}}\right)^{\frac{2}{3}}. \tag{55}$$

The total axial displacement is

$$\delta_a=\delta_1+\delta_2. \tag{56}$$

The static stiffness K_s is

$$K_s=\frac{dF_a}{d\delta_1}. \tag{57}$$

The dynamic stiffness K_d is

$$K_d=\frac{dF_a}{d\delta}. \tag{58}$$

The calculation process is shown in Fig. 5, where α^0 can be calculated according to the method in Reference [19].

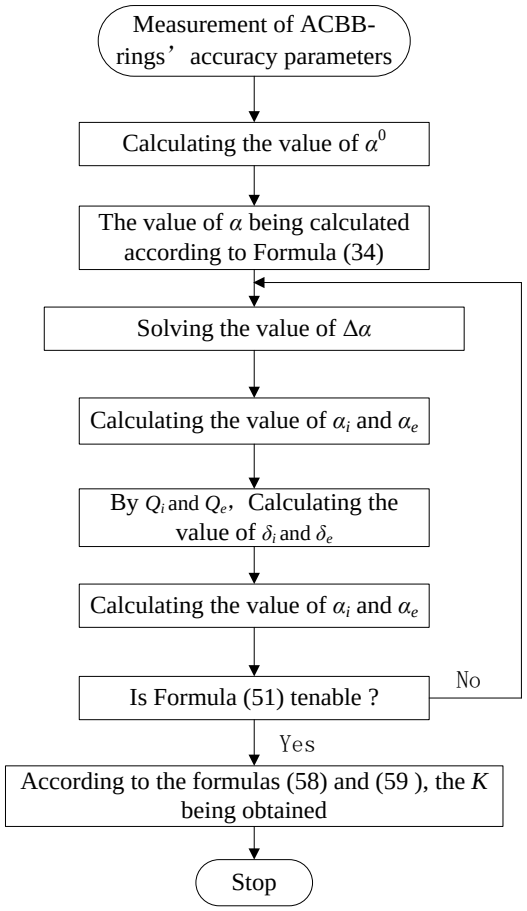

Fig. 5 Dynamic stiffness calculation flowchart of ACBB

2.5. Constraint conditions of designing main parameters

The design parameter constraint condition is defined in the high-speed ACBB design method, and the D_w constraint condition is

$$K_{wmin}(D-d)\le D_w\le K_{wmax}(D-d), \tag{59}$$

whereas

$$K_{wmin}=0.22 \tag{60}$$

$$K_{wmax}=0.32 \tag{61}$$

The constraint condition of N is

$$N\le\frac{\pi(D+d)}{2K_zD_w}, \tag{62}$$

whereas

$$K_z=K_{z1}+\frac{K_{z2}}{D_w}. \tag{63}$$

K_{z1} and K_{z2} satisfy

$$1.05\le K_{z1}\le 1.07, \tag{64}$$

$$1.2\le K_{z2}\le 1.5. \tag{65}$$

The constraint condition of d_m is

$$0.49(D+d)\le d_m\le 0.515(D+d). \tag{66}$$

The constraints of f_i and f_e are

$$0.515\le f_e\le 0.54,\quad 0.53\le f_i\le 0.58. \tag{67}$$

3. Case Analysis

Taking the 7006-ACBB as an example, the variation patterns between the main design parameters and the spin-roll ratio, rated dynamic load and stiffness are analyzed. The design parameters of the drawing are shown in Table 1.

Based on the constraint conditions and the high-speed ACBB design methodology, the possible

Table 1

Design parameters of 7006-ACBB, mm

Design parameter	D_w	N	d_m	R_e	R_i
Value	5.556	18	42.501~ 42.481	2.94~ 2.96	3.11~ 3.13

Table 2

D_w and N optional groups of 7006-ACBB unit, mm

	D_w	N
1	5.5	18
2	5.55625	18
3	5.95312	17
4	6	17
5	6.35	16
6	6.5	16
7	6.74688	15
8	7	15
9	7.14375	14
10	7.5	14
11	7.54062	14
12	7.9375	13
13	8	13

selections for the ball diameter D_w and the number of balls N (according to the maximum number of balls that can be accommodated) for the 7006-ACBB are presented in Table 2.

3.1. Analysis of spin-roll ratio

When calculating the spin-roll ratio, the preload $F_a \in [100, 140]$, N, d_m, R_e and R_i are used as variables respectively, D_w is constant, and the variation law of the spin-roll ratio is analyzed.

1. N is a variable. R_e is 2.95 mm, R_i is 3.12 mm, d_m is 42.491 mm, and the variation curve of spin-roll ratio is shown in Fig. 6.

2. R_i is a variable. R_e is 2.95 mm, N is 18, d_m is 42.491 mm, and the spin-roll ratio curve is shown in Fig. 7.

3. R_e is a variable. R_i is 3.12 mm, N is 18, d_m is 42.491 mm, and the spin-roll ratio curve is shown in Fig. 8.

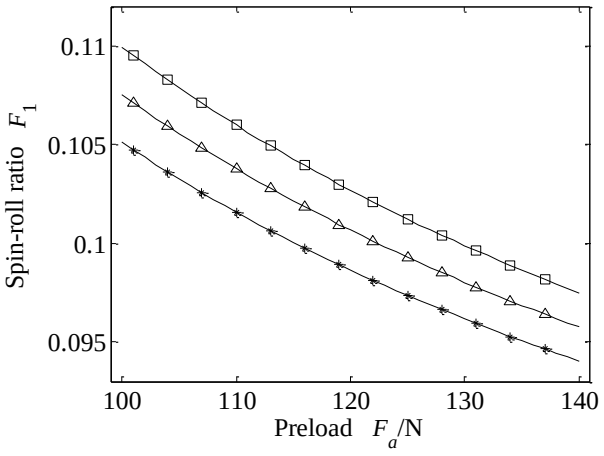

Fig. 6 Variation curve of N-F_1: * – N is 16, △ – N is 17, □ – N is 18

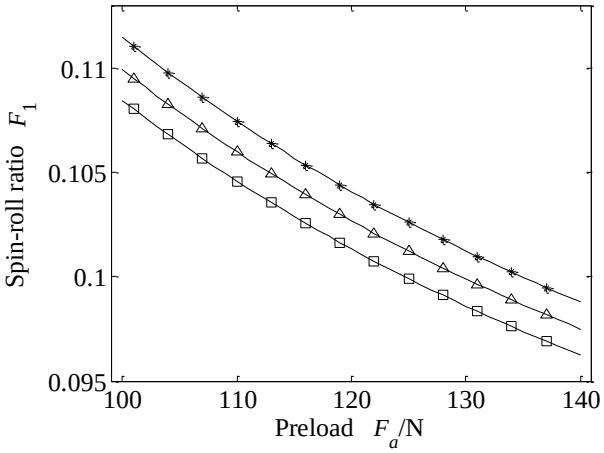

Fig. 7 Variation curve of R_i-F_1: * – R_i is 3.11 mm, △ – R_i is 3.12 mm, □ – R_i is 3.13 mm

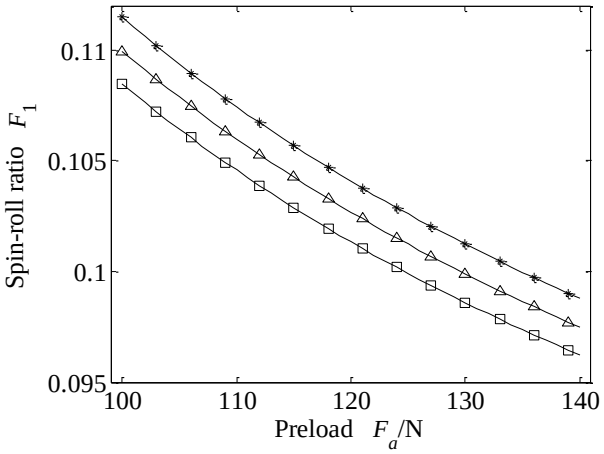

Fig. 8 Variation curve of R_e-F_1: * – R_e is 2.94 mm, △ – R_e is 2.95 mm, □ – R_e is 2.96 mm

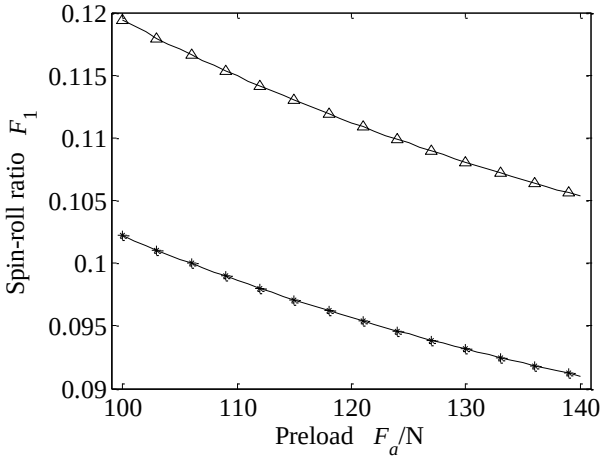

Fig. 9 Variation curve of d_m-F_1: * – d_m is 42.489 mm, △ – d_m is 42.4935 mm

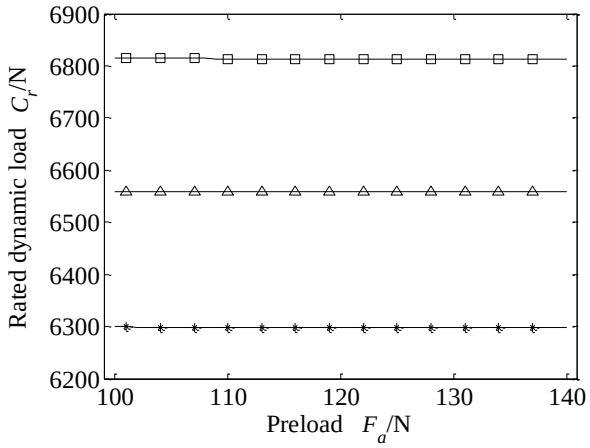

a

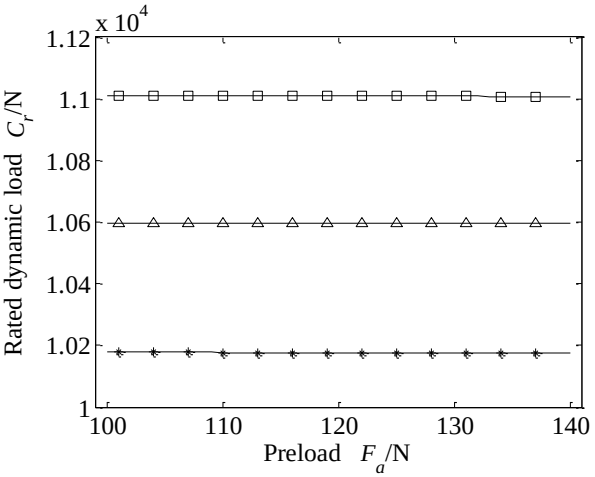

b

Fig. 10 Variation curve of N-C_r: a – ZYB, b – ISO; where: * – N is 16, △ – N is 17, □ – N is 18

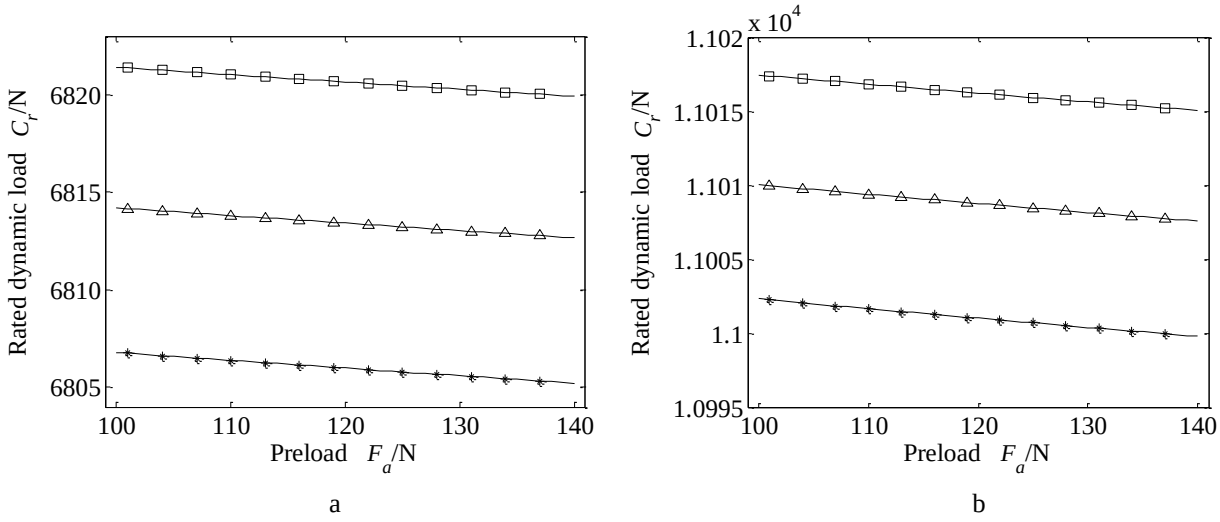

Fig. 11 Variation curve of R_i-C_r: a – ZYB, b – ISO; where: * – R_i is 3.11 mm, △ – R_i is 3.12 mm, □ – R_i is 3.13 mm

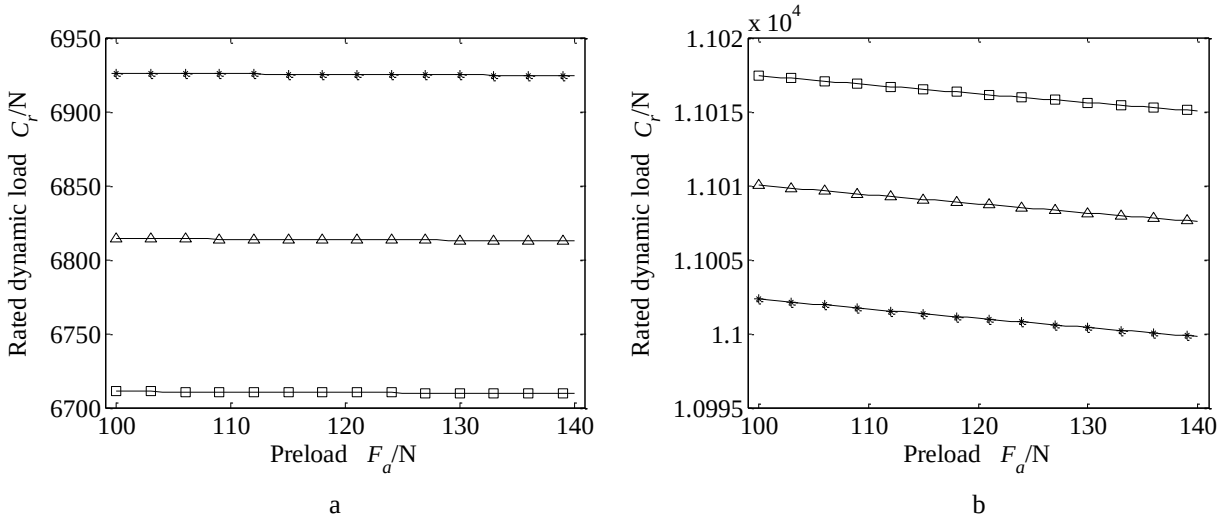

Fig. 12 Variation curve of R_e-C_r: a – ZYB, b – ISO; where: * – R_e is 2.94 mm, △ – R_e is 2.95 mm, □ – R_e is 2.96 mm

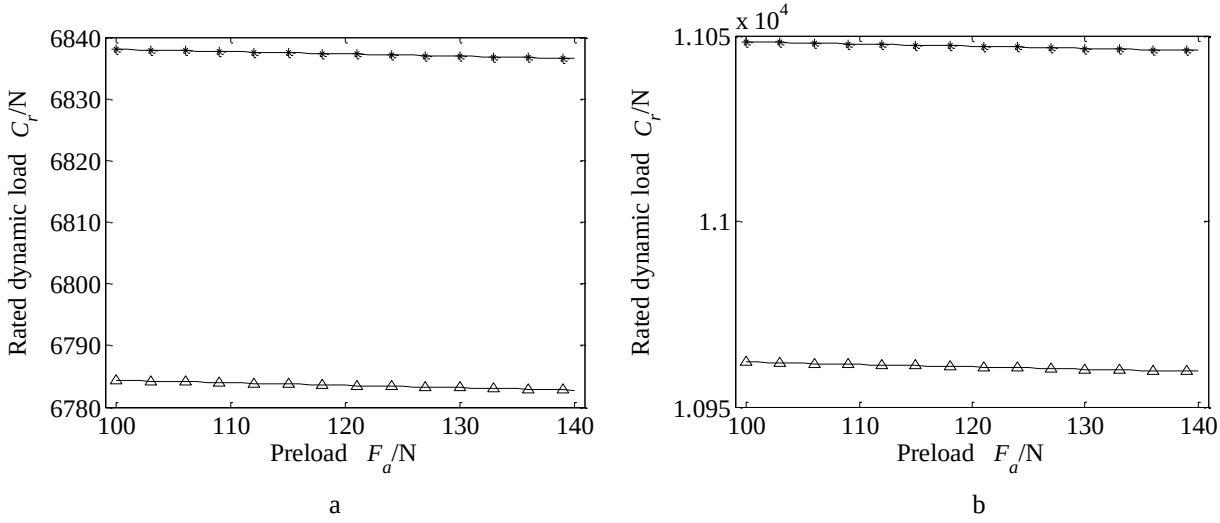

Fig. 13 Variation curve of d_m-C_r: a – ZYB, ISO; where: * – d_m is 42.489 mm, △ – d_m is 42.4935 mm

4. d_m is a variable. R_i is 3.12 mm, N is 18, R_e is 2.95 mm, and the spin-roll ratio curve is shown in Fig. 9.

3.2. Analysis of rated dynamic load

The rated dynamic load discussed is the radial basic rated dynamic load C_r, which is calculated by the methods in ZYB and ISO [17] respectively. N, d_m, R_e and R_i are still used as variables, and the preload $F_a \in [100,140]$ is used to analyze the variation law.

1. N is a variable. R_e is 2.95 mm, R_i is 3.12 mm, d_m is 42.491 mm, and the rated dynamic load change curve

is shown in Fig. 10.

2. R_i is a variable. R_e is 2.95 mm, N is 18, d_m is 42.491 mm, and the rated dynamic load change curve is shown in Fig. 11.

3. R_e is a variable. R_i is 3.12 mm, N is 18, d_m is 42.491 mm, and the rated dynamic load change curve is shown in Fig. 12.

4. d_m is a variable. R_i is 3.12 mm, N is 18, R_e is 2.95 mm, and the rated dynamic load is shown in Fig. 13.

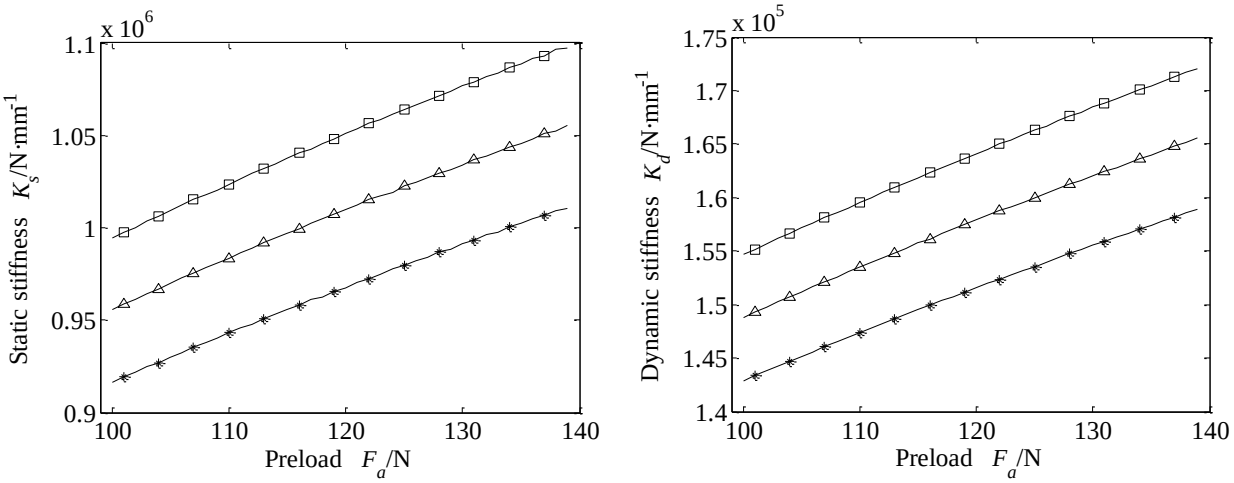

a b

Fig. 14 Variation curve of N-$K_{s,d}$: a – K_s, b – K_d; where * – N is 16, △ – N is 17, □ – N is 18

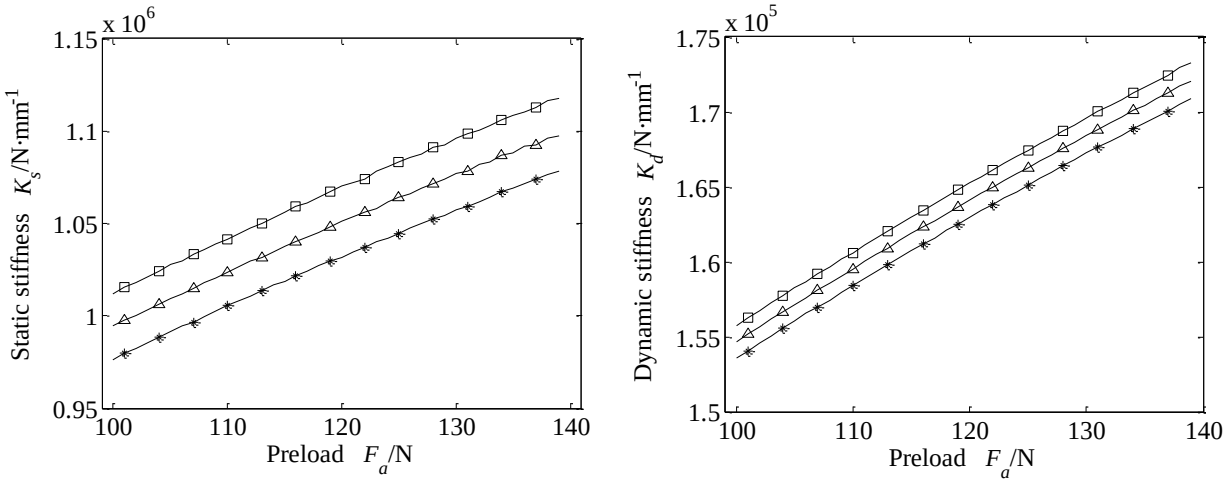

a b

Fig. 15 Variation curve of R_i-$K_{s,d}$: a – K_s, b – K_d; where: * – R_i is 3.11 mm, △ – R_i is 3.12 mm, □ – R_i is 3.13 mm

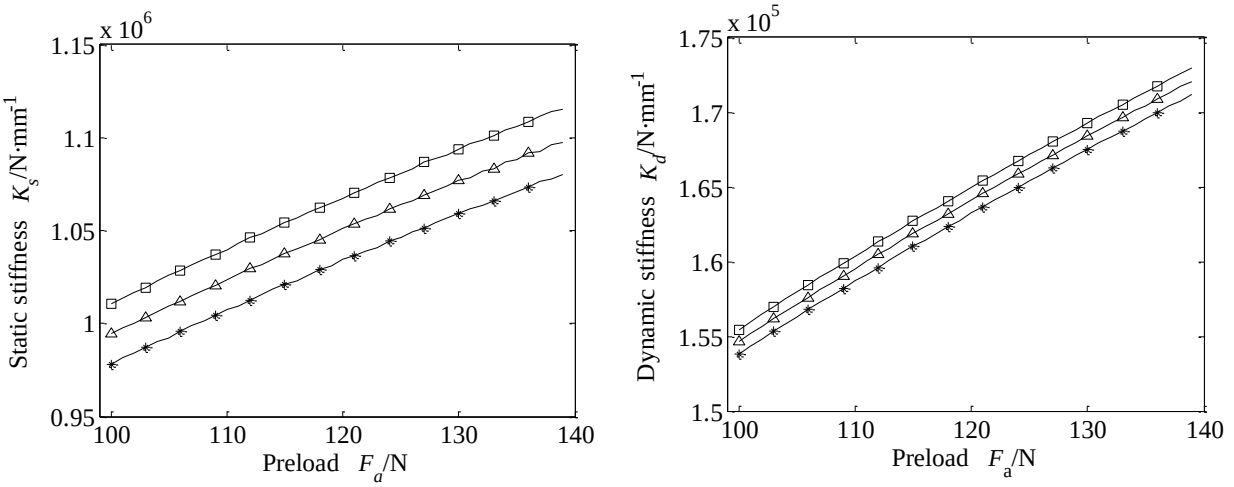

a b

Fig. 16 Variation curve of R_e-$K_{s,d}$: a – K_s, b – K_d; where:* – R_e is 2.94 mm, △ – R_e is 2.95 mm, □ – R_e is 2.96 mm

3.3. Analysis of stiffness

Compared with the spin-roll ratio and the rated dynamic load, the stiffness calculation is more complex and has many influencing factors. The definition of rolling bearing stiffness is also different from that of general mechanical structure stiffness. It refers to the external load required for the relative elastic displacement of the unit in the load direction of the inner and outer rings. In this section, N, d_m, R_e and R_i are also used as variables, and the preload Fa ∈ [100,140] is used to analyze the variation law.

1. N is a variable. R_e is 2.95 mm, R_i is 3.12 mm, d_m is 42.491 mm, and the stiffness is shown in Fig. 14.

2. R_i is a variable. R_e is 2.95 mm, N is 18, d_m is 42.491 mm, and the stiffness is shown in Fig. 15.

3. R_e is a variable. R_i is 3.12 mm, N is 18, d_m is 42.491 mm, and the stiffness is shown in Fig. 16.

4. d_m is a variable. R_i is 3.12 mm, N is 18, R_e is 2.95 mm, and the stiffness is shown in Fig. 17.

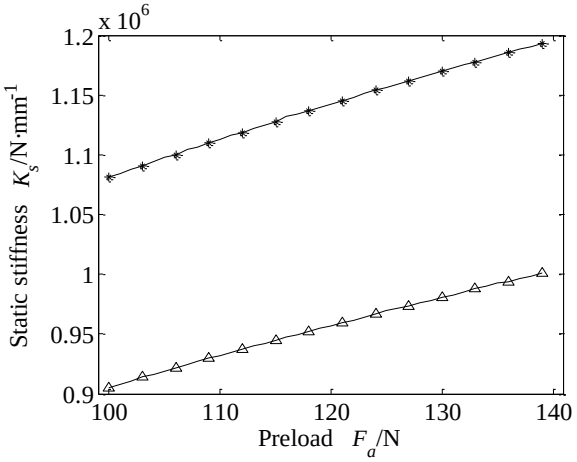

a

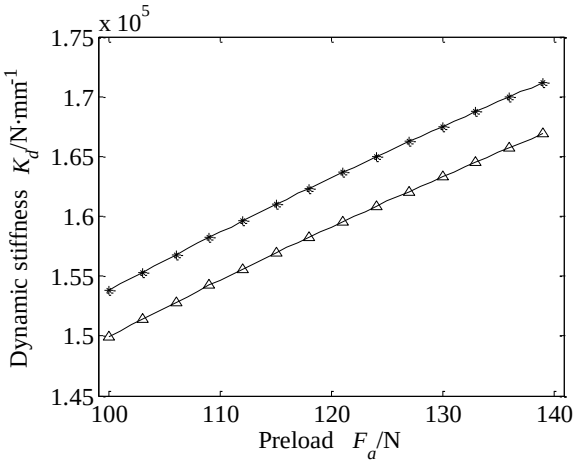

b

Fig. 17 Variation curve of d_m-$K_{s,d}$: a – K_s, b – K_d; where: * – d_m is 42.489 mm, △ – d_m is 42.4935 mm

4. Conclusions

In this study, the spin-roll ratio, rated dynamic load and stiffness are taken as the optimization objectives, and 7006-ACBB is selected as the research object. The variation law between the design main parameters and the objective function is analyzed. The specific work and conclusions are as follows:

1. According to the motion characteristics of ACBB at high speed, a formula for calculating the dynamic stiffness of high-speed ACBB is derived. The model does not introduce the influence of lubrication and other conditions on the motion, and considers the friction between the ball and the channel. The form is simple and the results can be obtained quickly, which is convenient for application in engineering.

2. The spin-roll ratio decreases with the increase of F_a; reducing the number of balls, appropriately increasing R_i, R_e or decreasing d_m can reduce the value of the spin-roll ratio, where d_m is determined by d_i and d_e. The decrease of the spin-roll ratio is beneficial to reduce the friction and heat between the ball and the ring. The stiffness increases with the increase of F_a, increasing the N, appropriately increasing R_i, R_e or decreasing d_m can increase the stiffness. According to the design method, more combinations of D_w and N can be selected, and the other four main parameters are related to D_w. It can be considered that selecting different D_w is equivalent to redesigning the bearing. When designing, the selection of D_w does not strictly follow the design method. Therefore, different D_w design schemes need to bring the design parameters into the objective function and determine the design scheme according to the calculated values.

3. The rated dynamic load decreases with the increase of F_a; increasing the N, appropriately increasing R_i or decreasing d_m can increase the rated dynamic load. According to ISO calculation, increasing R_e is beneficial to increase the rated dynamic load. In contrast, the ZYB calculation method yields opposite results. This discrepancy occurs because:

- The ISO method does not explicitly incorporate f_i and f_e.
- The ZYB method directly includes f_i and f_e, resulting in more comprehensive considerations.

4. The static stiffness and dynamic stiffness values are quite different, but the variation law with the design parameters is consistent.

It should be further clarified that the calculation results contain certain errors and should not be interpreted as absolute quantitative values. Instead, the focus should be placed on understanding the variation patterns between design parameter changes and optimization objectives. The research findings can provide valuable guidance for determining the main design parameters and controlling manufacturing process parameters.

Acknowledgements

The work is sponsored by Henan Key Laboratory of Green Building Materials Manufacturing and Intelligent Equipment.

References

1. **Deb, K**. 2001. Multi-objective optimization using evolutionary algorithms, Chichester, U.K.: John Wiley. 536p. https://dl.acm.org/doi/10.5555/559152.
2. **Choi, D. H.; Yoon, K. C.** 2001. A Design Method of an Automotive Wheel-Bearing Unit With Discrete Design Variables Using Genetic Algorithms, ASME Journal of Tribology 123(1): 181-187. https://doi.org/10.1115/1.1329878.

3. **Gupta, S.; Tiwari, R.; Nair, S. B**. 2007. Multi-objective design optimization of rolling bearings using genetic algorithms, Mechanism and Machine Theory 42(10): 1418-1443. https://doi.org/10.1016/j.mechmachtheory.2006.10.002.
4. **Li, T. J.; Zhu, C. S.; Lin-Fu, D.; Li-Guo, Z.; Xue-Ping, W.** 2010. Research on sensitivity of design parameters of rolling bearings, Journal of Shenyang University of Chemical Technology 24(2): 160-164.
5. **Cui, L.; Zheng, J. R.; Zhou, W.** 2012. Multi-objective optimization design for dynamic performances of ball bearings considering coupling effect of a rotor system, Journal of Vibration and Shock 31(24): 190-196. https://doi.org/10.13465/j.cnki.jvs.2012.24.018.
6. **Wu, L. S.; Liu, Z. Y.; Zhang, W.** 2006. Analysis on the Ratio of Revolution and Rolling of Angular Contact Ball Bearing for the High-speed Main Shaft of Machine Tool, Journal of Beijing University of Technology 32(8): 677-682.
7. **Yang, X. Q.; Jiang, S. F.; Chen, J. J.** 2000. Optimization design of high-speed angular contact ball bearing, Bearing (01): 1-5.
8. **Liu, S. C.; Wang, D. F. Shang, Q.; Yan, C.; Gao, X.** 2017. Multi-objective Optimization Design of High-Speed Grease-Lubricated Angular Contact Ball Bearings, Bearings 8: 1-5+10 (in Chinese). https://doi.org/10.19533/j.issn1000-3762.2017.08.001.
9. **Yun, X. L.; Mei, X. S. Jiang, G. D.; Li, Y.; Yuan, S.** 2019. Dynamic Stiffness Analysis and Testing Method of Angular Contact Ball Bearings for High-Speed Spindles, Journal of Vibration 39(04): 892-897+912 (in Chinese). https://doi.org/10.16450/j.cnki.issn.1004-6801.2019.04.030.
10. **Luo, T. Y.; Sun, D.** 2018. Optimal Design for Main Parameters of Angular Contact Ball Bearings Using Stiffness as Objective Function, Bearings (09): 1-3 (in Chinese). https://doi.org/10.19533/j.issn1000-3762.2018.09.001.
11. **Wang, D. F.; Fang, B.; Li, Q. R.; Zhang, J.** 2016. Calculation and Analysis of Stiffness for Angular Contact Ball Bearings, Bearings (04): 1-5 (in Chinese). https://doi.org/10.19533/j.issn1000-3762.2016.04.001.
12. **Wang, B. M.; Mei, X. S.; Hu, C. B.; Wu, Z. X.** 2010. Influence of inner ring centrifugal displacement on the stiffness of high-speed angular contact ball bearing, Jisuan Lixue Xuebao/Chinese Journal of Computational Mechanics, 27(1): 145-150.
13. **Singh, M.; Tiwari, R.** 2023. Design Optimization of Angular Contact Ball Bearing Using Genetic Algorithm and Grid Search Method, ASME Journal of Tribology 145(5): 054501. https://doi.org/10.1115/1.4056352.
14. **Abbas, M.; Metwalli, S.** 2025. Multi-Objective Optimization and Supervised Machine Learning for Synthesis of Rolling Element Bearing and Lubricant Selection, ASME Journal of Mechanical Design 147(12): 123501. https://doi.org/10.1115/1.4068662.
15. **Baklouti, A.; Dammak, K.; El Hami, A.** 2022. Optimum reliable design of rolling element bearings using multi-objective optimization based on C-NSGA-II, Reliability Engineering and System Safety 223: 108508. https://doi.org/10.1016/j.ress.2022.108508.
16. **Deng, S. E.** 2024. Principles of Rolling Bearing Design (3rd ed.), Beijing: China Standards Press.
17. ISO 281: 2007. Rolling bearings – Dynamic load ratings and rating life.
18. **Deng, S. E.** 2014. Principles of Rolling Bearing Design (2nd ed.), Beijing: China Standards Press.
19. **Ji, Y; Wang, D. F.; Xue, Y. J.; Zheng, H.; Han, T.** 2024. Dynamic accuracy's evolutionary regularity of angular contact ball bearing based on design parameters, Journal of Aerospace Power 39(6): 233-242. http://dx.doi.org/10.13224/j.cnki.jasp.20220389.

Y. Ji, K. Huang, H. Zheng, Y. Li, D. Wang, C. Gao, D. Sun

OPTIMIZATION DESIGN METHOD OF HIGH-SPEED ANGULAR CONTACT BALL BEARINGS

S u m m a r y

With the rapid development of high-speed rotating equipment technology, angular contact ball bearings (ACBBs) have been increasingly widely applied in industry. However, there is still a lack of systematic design theory support for their service performance under high-speed operating conditions. In existing engineering practices, the design of ACBBs often focuses only on a single performance index, such as rated dynamic load, spin-roll ratio, or static stiffness, with little consideration of the dynamic behavior changes caused by the ball "outward-thrown" under high-speed operation. To fill the above research gaps, this paper innovatively introduces dynamic stiffness as a key design index and proposes a comprehensive design method integrating spin-roll ratio and rated dynamic load. By establishing the kinematic model of balls in the raceway, the analytical relationship of the spin-roll ratio under high-speed steady-state conditions is derived; the applicability of different dynamic load rating calculation models is systematically compared, and a mathematical model of dynamic stiffness is constructed along with a numerical solution strategy. On this basis, the intrinsic laws governing the evolution of rated dynamic load, spin-roll ratio, and dynamic (static) stiffness with key design parameters are revealed. This study clarifies the coupling mechanism of key design parameters under high-speed conditions and establishes a parameter design strategy based on collaborative optimization. It provides a theoretical basis and methodological support for solving problems in engineering applications of high-speed ACBBs, such as inaccurate parameter selection and difficulty in ensuring dynamic performance. The research results help to further improve the design system of high-speed ACBBs and have important guiding significance for enhancing the design quality and service reliability of bearing products.

Keywords: angular contact ball bearing, stiffness, spin-roll ratio, rated dynamic load.

Received April 11, 2025
Accepted December 15, 2025